A Novel Release Mechanism Employing the Principle of Differential Coefficients of Thermal Expansion

Clint Apland*, David Persons*, David Weir*, and Michael Marley*

Abstract

APL has developed a novel miniaturized release mechanism that can be used in CubeSats, NanoSats and miniature space-borne science instruments. This miniature device is inexpensive, reusable, power-efficient, and doesn't consume any flight parts. The principle of operation for the release mechanism is to use two parts that have complementary coefficients of thermal expansion (CTE). Requirements, key challenges, performance results and lessons learned are presented. Results from a total of 37 test actuations of the design under various environmental conditions demonstrated a robust device that performed reliably in a flight-like environment.

Introduction

While in the process of developing the first 3U CubeSats designed and built at APL, the authors became convinced they needed a unique release mechanism for use in restraining and releasing the CubeSat's four solar array panels. Driven by power and volume limitations, the actuator developed in this original work is inexpensive, has a single moving part, generates no shock, uses little power, is re-settable, and does not consume any flight parts in its operation. In the process of qualifying the release mechanism, we revised the design twice to improve the performance, ease of operation and installation of the device, and to reduce the cost of producing the devices.

The CTE Release Actuator (CTERA) has successfully completed functional testing in vacuum, self-actuation testing and static load testing. It was tested under three power profiles representing those expected during flight. It has been tested in an actuator only configuration, as well as with a deployable structure representing a possible mission use.

The principle of operation for the release mechanism uses two parts that have complementary coefficients of thermal expansion (CTE). The material with a low CTE is inserted into a hole in the material with the high CTE after the high CTE material is heated. Once the high CTE part cools, the low CTE part is trapped due to an interference fit between the two parts. The interference is sized for the retaining force desired from the actuator. The low CTE part, called the plug, is fastened to the part or assembly to be separated from the space vehicle. When the high CTE part, called the cup, is re-heated, the low CTE part is freed, just as a bolt would be freed from a separation nut.

Key challenges for the design included analysis to set the machining tolerances required, choice of the mechanical surface properties of the two interfacing parts, finding low cost heaters with high watt-density that operate at low voltage, and testing various power profiles to minimize the power drawn by the device. A MathCAD design tool was developed for initial sizing of the interference fit, and later, using a test-verified release coefficient, to predict the release temperature under the influence of the kick-off spring.

* Johns Hopkins University Applied Physics Laboratory, Laurel, MD

Requirements

As the packaging layout of the reference mission progressed, these key requirements for the design of this tiny actuator became evident:

- Tiny envelope of less than 9.83 cm^3 (0.6 in^3) – the device needed to fit into an approximately 2.54 x 2.54 x 1.524 cm (1" x 1" x 0.6") envelope.
- Low power availability - Since power for the CubeSat reference mission was at a premium, we needed to minimize the amount of power drawn by the actuator. The conductive heat loss between the cup and the plug, as well as the cup and the spacecraft, was a priority.
- Low upper temperature limit – The avionics on the reference mission didn't have the capability to sense the temperature of the actuator; therefore we needed to use a set time for resistor power cutoff. This limitation forced the design to release at a much lower operating temperature in order to reduce the risk of damaging the resistor heating source.
- A relatively large holding capacity for the actuator's size – the load requirement with test factor of 1.5 was 143 N (32.25 lb).
- A tension-only boundary condition – due to the short distance from the hinge, a spherical ball boundary condition was needed, with no room for a spherical bearing.
- Low shock – The CubeSat specification prohibits pyrotechnic devices. APL also chose to minimize shock generated by the chosen release mechanism to protect CubeSat avionics and mechanisms. The CTERA produces negligible shock.
- Easily resettable – The device used in the APL CubeSat needed to be easy to reset. Removing the device from the SV for re-set would cause unacceptable delays in the I&T process.
- Use of non-magnetic materials throughout the mechanism.

Trade Study Results

We conducted a quick electrical characteristic comparison, shown in Table 1, between the CTE actuator and commercial devices, with a particular focus on the energy required to actuate them. The table shows five release actuators and their electrical characteristics. We did not attempt to differentiate mechanical characteristics, since only one other device in the table fits the size constraints to which the CTE actuator was designed.

Table 1 - Device Trade Study

Device	Current (A)	Voltage (V)	Power (W)	Resistance (Ω), Total	Δtime (s)	Energy (W-s)	% Battery Energy
Device #1 (SMA)	1.00	9.00	9.0	9	35	315	0.20%
Device #2 (SMA)	5.36	7.50	40.2	1.4	0.032	1	0.0008%
Device # 3 (Paraffin Initiated Actuator)	0.36	28.08	10.1	78	150	1516	0.94%
Device #4 (SMA)	3.50	14.70	51.5	4.2	0.035	2	0.0011%
APL CTE Actuator	2.60	7.28	18.9	2.8	17.8	337	0.21%

Device # 1 can be used in applications similar to those for which the CTE Actuator can be employed. This device has lots of heritage, produces almost no shock, and is a highly reliable device in APLs experience. Its nominal power performance is slightly better than that of the actuator. This device must be removed from the space vehicle (SV) or instrument to be re-set and it consumes notched bolts with each actuation. This particular model would need to have a custom heater resistance to be used on a CubeSat, since the 9-ohm resistive heater wouldn't dissipate enough power to actuate the device at minimum voltage (6V). This device, unless non-recurring engineering was expended to re-size it, simply would not fit in the volume allotted in the APL CubeSat.

Device #2 is another shape memory alloy device. This device uses a shape memory alloy to actuate a ball detent mechanism which releases a deployable item. Its load capacity is far beyond what is needed for many CubeSats or small instruments. It uses very little power and has an almost instantaneous actuation. It's also much larger and more massive than could be used in this APL CubeSat. It draws far more current than a CubeSat could supply without dedicated capacitor banks. While it produces much less shock than a pyrotechnic device, it still produces shock, which must be evaluated in the design process.

Device #3 uses a resistive heater that heats paraffin wax. When the wax is heated, it expands. The actuators are designed to produce linear motion with a defined output force. They are compact, highly reliable, and insensitive to contamination. They require a companion mechanism to affect the release of a deployable device. They consume much more energy than any other device compared.

Device #4 uses shape memory alloy wires to rotate a cam which allows a four segment nut to separate and release a bolt. They have a much higher load capacity than is needed for the reference application. They use very little energy and are near-instantaneous actuators. They are much larger and massive than could be used in this APL CubeSat. They draw much more current than is available in a CubeSat.

Prior to conducting the trade study, we eliminated pyrotechnic actuators from consideration, because the CubeSat specification forbids their use. We also considered two other custom designs, one that operated by cutting 'fishing line' and the other that operated by vaporizing a Ni-Chrome wire. Enough work was completed on each design to determine that for the particular combination of available volume, power and holding force of this application, the designs were overly complex and difficult to manufacture and assemble. We conducted creep testing on available polymer lines compatible with a low power line cutter, and concluded that the lines' creep would result in loss of preload in the restraint, causing gapping and unacceptably high loads during flight. We also had contamination concerns arising related to melting plastic and its possible re-solidification on solar array cells or optical surfaces. While promising, given a different situation, these ideas were eventually shelved for this application.

Design Function & Development

The **first generation device** (Figure 1) used parts without any surface coatings and used a single 30-W thick film power resistor as the heater element. It served as a proof-of-concept, but was not suitable for flight use. The outer cup was fabricated from 6061-T6 aluminum, the inner plug from 6AL4V titanium. The machining tolerances for the cup (high CTE) and plug (low CTE) parts were critical, since the interference fit between the two was just 15 µm (0.0006"), nominal OD to ID. Because of this, we machined the parts to a diametrical tolerance of 3.81 µm (± 0.00015"). A simple tension-only test stand was used for testing the single first generation prototype. The first generation actuator consisted of an un-plated aluminum body fabricated on a manually operated lathe, and single 30-W 3-Ω thick film resistor, an interface plate with fiberglass thermal insulators, and an un-plated titanium plug.

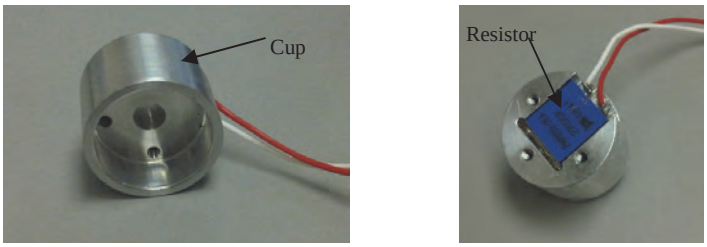

Figure 1 – First generation device with a bare aluminum body and a single 30-W resistor

The **second generation device** featured redundant heaters, a kick-off spring and a vent hole, and is depicted in Figure 2. The heaters have a temperature limit of roughly 135°C at our highest operating current, and the operating range of the actuator needed to be well below this temperature during operation. Our reference mission didn't have the capability to sense the temperature of the actuator (this

was a self-imposed limitation implemented early in the program and will be reversed in future CubeSats); therefore we needed to design for a much lower operating temperature to reduce the risk of damaging the resistors. We therefore chose to limit the operating temperature to 115°C. In practice, actuation temperatures rarely reach 115°C, but setting the actuators for flight gets much easier as the temperature increases. The aluminum cup is thermally isolated from the host structure with G-10 isolators to minimize heat loss and the overall power needed to actuate the device. We are exploring the idea of coating the flight actuators with low emissivity coatings to reduce power required for actuation by limiting heat loss due to thermal radiation.

The aluminum parts are plated with a hard coat anodize treatment, but the titanium parts were left bare. The device acted as its own tell-tale separation indicator. When the plug is fully seated in the cup, it contacts the kick-off spring, which is electrically connected to the cup. A circuit is completed from the CubeSat input-output card through the CTERA and its titanium plug, through the solar array substrate, back over the solar array hinge line, into the CubeSat harness into the IO card. When the plug is released, continuity is broken, indicating separation. We verified the concept through several cycles of operation on the tension-only test-stand. The design required great care to re-set. The single-piece plug needs to be precisely aligned with the cup, inserted in as short a time as possible to reduce plug heating. This second-generation design also required fighting against a 44.5-N (10-lb) kickoff spring force during insertion. We ended up galling the surface of the plugs in our efforts to accomplish this. The second generation device functioned unreliably in flight-like use with a solar array wing. The flight-like wing, with its hinge line parallel to the gravity vector, imposed side loads upon the release mechanism that the test stand did not.

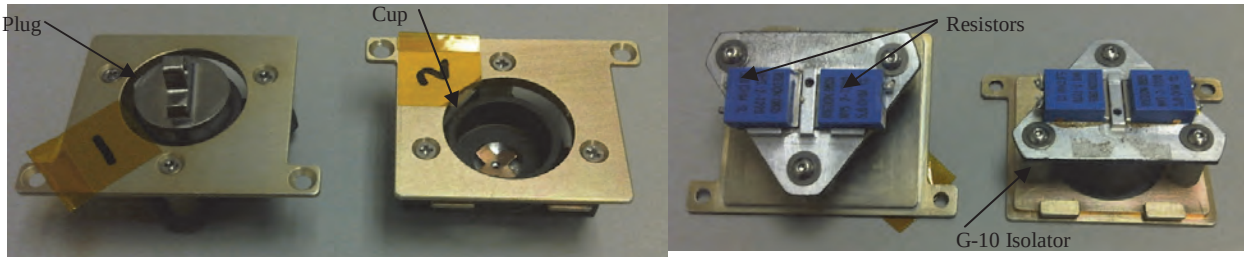

Figure 2 – Underside (left) and top side (right of the second generation device)

The **third generation device** featured a lower mass high CTE part, a reduced length interface between the two materials, and less heat transfer between the high CTE and low CTE parts, and surface treatments on both of the mating parts. Elimination of the kickoff spring preload during the precision mate of the high and low CTE parts made the mechanism much easier to re-set. Redesign of the solar array fitting accommodated the range of motion constraints imposed by the flight solar array wing by using a custom 'near-spherical bearing' featuring a pin and dual conical hole. The new interface to the reference mission solar array wing allows more alignment adjustability between the wing and the actuator. This tolerance eliminates racking and binding during wing deployment. Figure 3 depicts the third generation actuator body and plug and the assembly of pin, lower interface bracket and plug cap. The space-saving pin and dual cone features provide 'near spherical bearing' behavior in much less volume. To minimize galling and cold welding the aluminum and titanium parts under a sustained 6.9 mPa (1000 psi) interface pressure, surface finishes were critical. Two versions were fabricated, featuring different combinations of surface treatments on the high and low CTE materials. Some limited functional testing was used to determine which surface treatment combination would be used for the final design. Metrics were part wear, the change in temperature required to achieve separation, and the electrical energy expended to achieve separation. We selected hard coat anodize for the aluminum parts, and Tiodize, Type 2 for the titanium parts. Reduction of the contact area between plug and cup significantly reduced the amount of energy required for the actuator to function. Additionally, the annular interface area between the bottom of the plug and the cup was reduced by the addition of 8 radial ridges, which dramatically reduce the amount of heat transfer between the cup and the plug. Reducing energy absorbed by the plug reduces the amount of delta-T required to separate the plug from the cup. Because of the solar array deployed

geometry, the hinge causes each of the panels to deploy 90 deg and to twist 45 deg in an axis normal to the initial deployment axis.

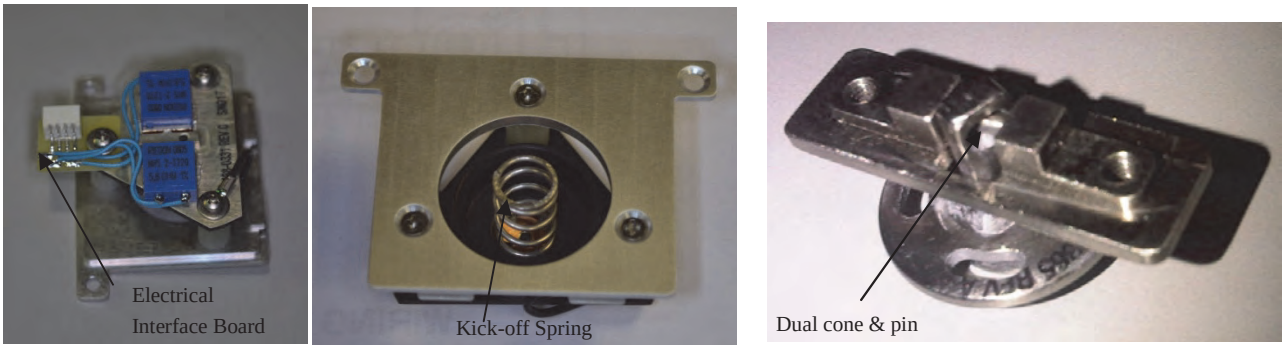

Figure 3 – Third generation actuator showing interconnect PC board, tell-tale harness, kickoff spring and retainer, and upper interface assembly with "near spherical bearing"

Because of this and because of the small radius the plug travels during deployment, the second-generation actuator had the tendency to bind during deployment. The reduction of the cylindrical interface area between the cup and plug reduced the likelihood of binding due to any lateral load or misalignment during actuator release. Binding was also reduced by changes to the lead in angles on the outer diameters of the cup and plug. The taper on the inner diameter of the plug reduces the probability of the cup hanging on the kick-off spring during deployment. The change to a two-piece plug, consisting of an annular plug with a cap allows insertion of the plug without compressing the kick-off spring. This eliminates the possibility of binding and galling while setting the actuator for flight, greatly facilitating reassembly. Figure 4 shows some of the features of the third generation actuator.

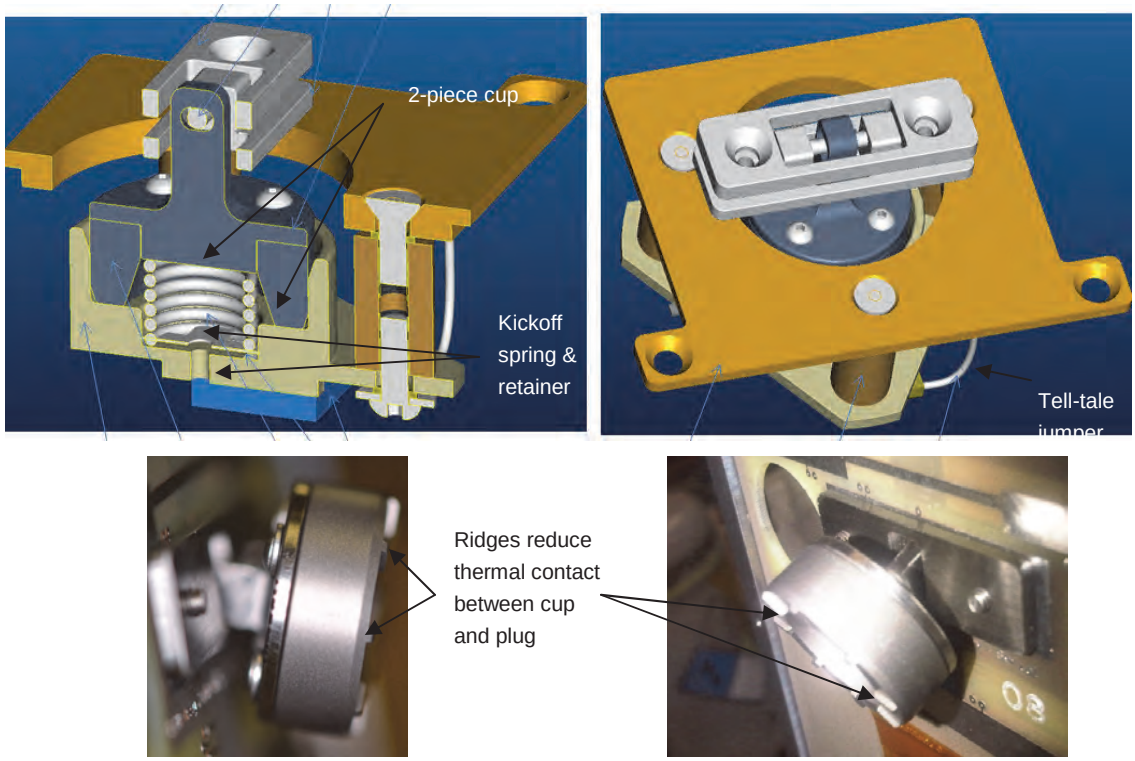

Figure 4 – Four views of the third generation device.

Testing Results & Data Analysis for Each Generation

First Generation

The primary intention of the first round of testing was to verify our assumptions about the electrical and thermal aspects of the concept. The device would eventually reach the temperature we calculated was required for separation (approximately a 70°C delta), but we learned that a single 30-W device was insufficient in both power handling capacity and output power. The power output was considered insufficient because it took several minutes for the device to change temperature. We theorized that more power input would reduce the delta-T of the low CTE plug part, as increasing the temperature of the high CTE part faster would provide less time for heat transfer to the low CTE part. This would, in turn, require a lower delta-T in the high CTE part to achieve separation. This was proven later in modifications implemented in the third generation device. We consulted with electrical component engineers who helped us pick parts using appropriate levels of part de-rating. Before this, we failed a few resistors by running them above their current-temperature curves. Using appropriate de-rating guidelines, we increased the resistance to 5.6 Ω, doubled the number of resistors, and switched from 30-W parts to 50-W parts. After the intial thermal and electrical tests were complete, we verified that concept would work, as we were able to expand the aluminum part to the point that we were able to assemble the unit. When we performed the first simulated actuation by removing the plug from the actuator at ambient pressure, we realized we had forgotten a vent hole in the actuator body. We also learned that we couldn't make the parts on a manually operated lathe. We needed a CNC lathe to achieve the required tolerances for consistent device operation. The first generation test rig is depicted in Figure 5.

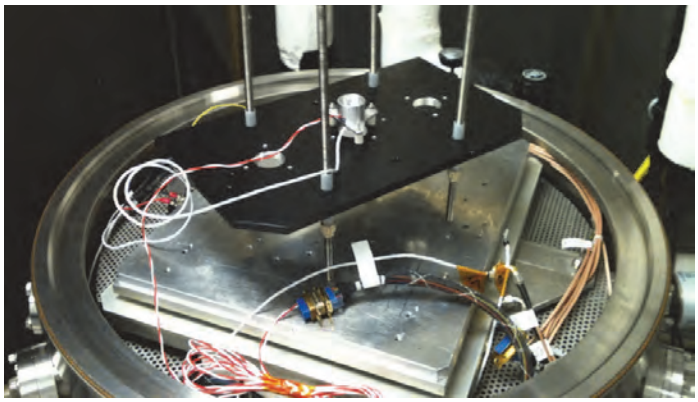

Figure 5 - First generation device shown in a bell jar type vacuum chamber. Striped wires are power, white wires are temperature sensors.

Second Generation

The second generation of the actuator was subjected to the tests listed below. Static load testing was conducted prior to functional testing on the actuator, and a load of 334 N (75 lb) was maintained for 15 minutes. Following static load testing, we performed several separations at ambient conditions with 2 A of current. As expected, it took a long time to separate (236 sec). The delta-T to separate was low, 66°C, which we think can be attributed to the virgin state of the actuator (blemishes accrue with uncoated parts). Initial functional testing at vacuum was then successfully completed (separations 4 and 5). Lastly, 12 separations were conducted in vacuum under flight conditions, with the results summarized in Table 2.

Run 15 was a scrub. Power was cut off before the full actuation occurred. Note 4 indicates a smooth plug insertion. Note 5 indicates a rough plug insertion. Nine of the twelve separations can be considered to be in family with the majority of the sample population. There were three separations that were out of family. We think these three separations took longer because the insertion of the plug into the cup for these runs was rougher. The rough insertions likely were due to a misalignment of the parts. As the number of cycles increased, we noted some wear marks forming on the uncoated titanium part, indicating that some galling took place, primarily during insertions, but during ejection, as well.

Table 2- Test data from second generation actuator.

Test #	Vacuum (Torr)	Current (A)	Voltage (V)	Power (W)	Tamb (°C)	Trel (°C)	ΔT (°C)	Δtime (s)	ΔT/Δt	Energy (W-s)	% Batt Energy	Note
4	2.50E-01	2.00	5.60	11.2	19.1	94.0	74.9	147	0.51	1646	1.02%	5
11	2.50E-02	2.16	6.05	13.1	23.6	94.0	70.4	100	0.70	1306	0.81%	4
17	2.50E-02	2.16	6.05	13.1	23.6	93.6	*72.0*	100	0.72	*1320*	0.82%	4
12	2.50E-02	2.16	6.05	13.1	21.1	104.0	82.9	123	0.67	1607	1.00%	5
18	2.50E-02	2.16	6.05	13.1	19.3	91.0	71.7	115	0.62	1502	0.93%	4
5	2.50E-01	2.58	7.22	18.6	24.0	87.8	63.8	70	0.91	1305	0.81%	4
6	2.50E-02	2.60	7.28	18.9	18.5	92.0	73.5	68	1.08	1287	0.80%	5
7	2.50E-02	2.60	7.28	18.9	18.9	89.2	70.3	66	1.07	1249	0.77%	4
8	2.10E-02	2.60	7.28	18.9	19.5	100.3	80.8	69	1.17	1306	0.81%	5
9	2.10E-02	2.60	7.28	18.9	20.0	90.2	70.2	62	1.13	1174	0.73%	4
10	2.50E-02	2.60	7.28	18.9	23.5	91.0	67.5	61	1.11	1155	0.72%	4
13	2.50E-02	3.02	8.46	25.5	18.9	88.7	69.8	46	1.52	1175	0.73%	5
14	2.30E-02	3.02	8.46	25.5	19.9	80.2	60.3	39	1.55	996	0.62%	4
16	2.50E-02	3.02	8.46	25.5	23.8	80.6	56.8	38	1.49	970	0.60%	4
	Not a “standard” power case.											
	Low power case											
	Nominal Power Case											
	High Power Case											
	Outlier											

We performed a preliminary analysis of only the separations performed in vacuum. A B-basis time to separate was calculated for the whole data set, and each of the three battery state of charge cases. The B-basis time to separate was calculated as follows: $\mathbf{T_{2\sigma} = Mean + (2 * \sigma)}$ where $T_{2\sigma}$ is the 2 sigma time to separate, ***Mean*** is the arithmetic mean of the times to separate, and σ is the standard deviation between the times to separate. Table 3 lists the data for the four cases analyzed (all vacuum separations, nominal power, high power, low power).

Table 3 - Second generation statistical results.

Data Set	Mean Time to Separate	Standard Deviation	2-sigma time to separate
All vacuum	78.86	33.04	144.94
Nominal (2.6A)	65.2	3.56	72.33
Low (2.16A)	109.5	11.45	132.39
High (3.06A)	41	4.36	49.717

The lessons learned from the 2nd generation testing were:

- This version of the actuator was too difficult to set for flight. The operator was required to precisely align the plug in the cup and then to insert it into the cup with enough force to overcome the preload spring. Having to push the plug into the cup with force makes the actuator too susceptible to galling.
- Performance degrades over time because of galling produced during resetting operations. Both high pressure surfaces needed to be hard coated.
- The actuator was susceptible to racking when coupled with the reference mission solar array engineering model.

- The amount of energy required for release needed to be further minimized for the 3rd generation design.
- The tell-tale function of the actuator was determined to be reliable through all testing.
- Installation of the plug is critical to the consistent operation of the actuator. We determined to make insertion easier and more repeatable by a redesign that eliminated the preload spring force during insertion.
- Use the highest possible insertion temperature during assembly.

Third Generation

The first 4 units fabricated were fabricated to select which actuator coatings should be employed for follow-on use of the actuators fabricated for flight. Actuator SN002 featured Chemical Conversion Coating (MIL-C-5541, Class 3) coating on the aluminum cup part and Tiodize, Type II (AMS-2488, Type 2) on the titanium plug part. For SN002 (Engineering Model), we conducted 7 separations, and then we retired the unit.

Actuator SN004 featured Hard Coat Anodize (MIL-A-8625, Type 3) on the aluminum cup part and Tiodize, Type II (AMS-2488, Type 2) on the titanium plug part. We conducted 6 separations, the self-actuation test, the static load test, and 2 more actuations. The third generation tests used an engineering model CubeSat solar array to represent the correct boundary conditions for the device. Figure 6 depicts the solar array wing and test fixture. The SN004 actuator had much better performance, and its tolerances and coating combination were selected for the final design.

We characterized performance of the SN004 actuator in the following sequence:

- A single functional test at ambient conditions to verify workmanship (test 4.1). Time and delta-T were recorded for all functional tests.
- Two separations in vacuum at nominal power (tests 4.2 and 4.3).
- A separation in vacuum at high power (4.5).
- A separation in vacuum at low power (4.6).
- A self-actuation test to determine the maximum temperature the actuator can be exposed to without spontaneously actuating (4.7). Temperature at separation was recorded.
- A static load test to verify that the actuator can withstand launch loads. Time and load were recorded (4.8).
- Two separations in vacuum at nominal power to verify that the device was not affected by the static loads test (4.9 and 4.10).

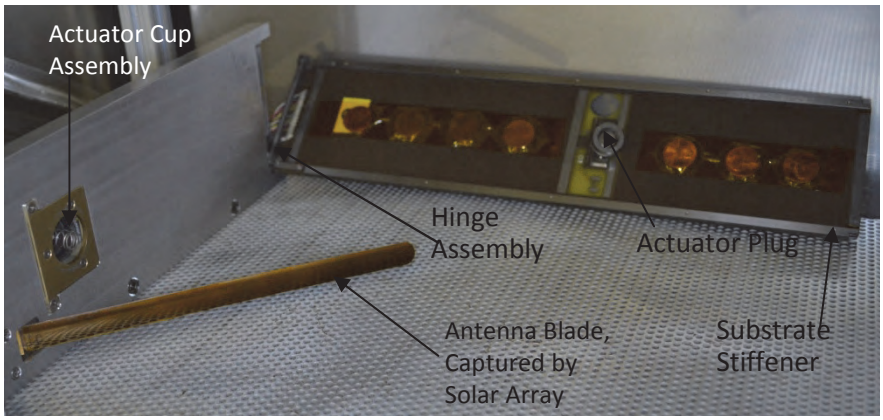

Figure 6 – The solar array wing and test fixture duplicated the boundary conditions for flight actuator testing.

The test at ambient conditions verified that workmanship was acceptable. The two tests at ambient temperature in vacuum showed the expected reduction in delta-T and time to separate. These results also showed (despite the small number of tests) a tight data grouping, showing that the device is repeatable. The tests at 3 A and 2.16 A showed that, as expected, the time to separate is inversely proportional to input current, when the tests are run at the same initial temperature. Somewhat surprisingly, the delta-T for the 2.16 A case was lower than those of the 2.6-A cases. Figure 7 shows the test stand inside the vacuum chamber.

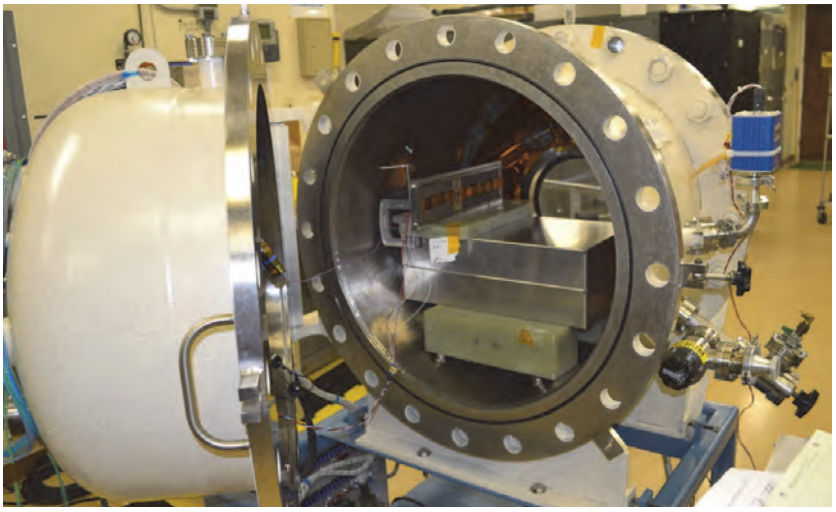

Figure 7 – Test stand, actuator and CTERA shown in vacuum chamber.

Following the tests at 2.16 A and 3 A, we conducted the self-actuation test. The purpose of the self-actuation test was to determine the temperature at which the actuator would release a deployable structure while unpowered. The actuator was required to reach a temperature higher than 50°C before self-actuating to demonstrate a 10°C temperature margin. The ambient pressure temperature cycling chamber was set to ramp temperature at a rate of 1°C per minute, starting at room temperature, which was approximately 19°C. We monitored the tell-tale circuit until the device actuated at 65.9°C. The highest predicted temperature for the CubeSat prior to solar array deployments is 40°C, which gives a margin of 25.9°C on self-actuation.

Following the self-actuation test, we conducted a static loads test. The purpose of the static load testing was to determine if the selected coatings and tolerances of the serial number 004 actuator can withstand launch loads after 7 separations. Note that the interference fit for the actuator tested, SN 004, is significantly smaller than those of the flight devices (SN 011-018). Since holding capability is a function of the interference fit, the flight actuators are able to react more load than the SN 004 device. The fixture used for static load testing is depicted in Figure 8. Tension on the actuator was increased in ¼ load increments and held for at least 30 seconds until the final load of 160 N (36 lb) was reached. Load was maintained at or above 156 N (35 lb) for 5 minutes. Following the static loads test, the CTERA was cycled two more times at ambient temperature and nominal power in vacuum (tests 4.9 and 4.10). Results from these two tests indicated that the electrical and thermal performance of the device wasn't affected by the static loads test. Results from tests 4.2, 4.3, 4.9 and 4.10 are tightly grouped. The raw data from the tests are presented in Table 4

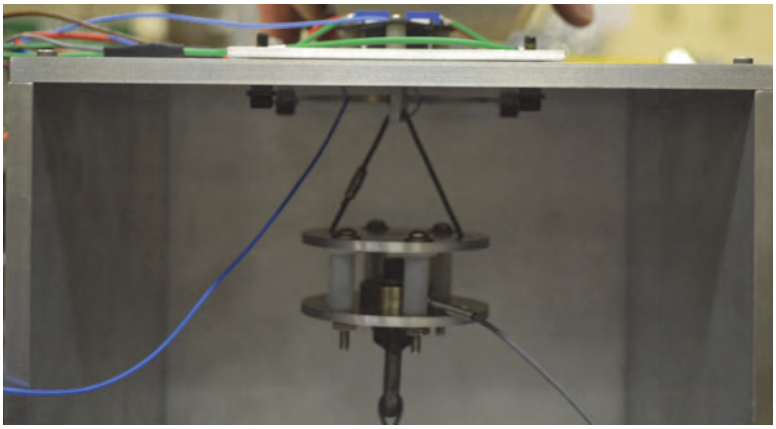

Figure 8 – The CTERA withstood 1.5 times the maximum expected flight load for 5 minutes.

Table 4 - Non-flight third generation actuator data, SN 004.

Test #	Vacuum (Torr)	Current (A)	Voltage (V)	Power (W)	Tamb (°C)	Trel (°C)	ΔT (°C)	Δtime (s)	ΔT/Δt	Energy (W-s)	% Batt Energy	Interference Fit	Note
4.1	ATM	2.60	7.28	18.9	19.5	71	51.5	33	1.56	625	0.39%	0.0003	
4.2	2.50E-02	2.60	7.28	18.9	18.7	45.0	26.3	18.5	1.42	350	0.22%	0.0003	
4.3	2.50E-02	2.60	7.28	18.9	18.5	44.0	25.5	18	1.42	341	0.21%	0.0003	
4.9	2.50E-02	2.60	7.28	18.9	18.4	47.8	29.4	17	1.73	322	0.20%	0.0003	1
4.10	2.50E-02	2.60	7.28	18.9	18.5	46.0	27.5	17.5	1.57	331	0.21%	0.0003	1
4.5	2.50E-02	3.02	8.46	25.5	18.5	39.8	21.3	12	1.78	306	0.19%	0.0003	
4.6	2.50E-02	2.16	6.05	13.1	18.8	42.2	23.4	26	0.90	340	0.21%	0.0003	
4.4	7.55E+02	2.60	7.28	18.9	UNK	UNK	UNK	UNK	UNK	UNK	UNK	0.0003	*2*
4.7	7.55E+02	0.00	0.00	0.0	18.9	65.9	47.0	NA	NA	NA	NA	0.0003	3
4.8	7.55E+02	0.00	0.00	0.0	19.0	NA	NA	NA	NA	NA	NA	0.0003	4

1	After static load test.
2	Actuated while adjusting current delivered to the resistor. At ambient. No data recorded.
3	Will not self actuate until ~66°C. SV will not go above 40°C. Adequate margin.
4	Static Load Test. Requirement (with test factor 1.5) was 143.5N (32.25#). Held above 157N (35.3#) for 5 minutes.

When the results from SN 004, with AMS-2488, Type 2 coating for titanium and hard coat anodize coating for the aluminum were compared to those for SN 002, with the same titanium finish and chemical conversion coating (MIL-C-5541, Class 3) of the aluminum, the SN 004 device was the clear winner.

SN 002 was tested first, and we concluded testing after the first 7 cycles because the data were poorly grouped, the performance of the device was perceptibly deteriorating, and we observed increasing damage to the interfacing surfaces of the aluminum and titanium parts. SN 002 raw data are not presented due to space restrictions.

Once the final design was selected, we fabricated eight flight units and conducted the following tests in the following order to validate the design. The flight mechanisms (SN 011 through 018) underwent the following testing to further validate the design and workmanship, and the raw data from these tests are presented in Table 5:

- At least one separation at nominal current at ambient temperature in vacuum (for SN 011-018, green shaded portion of the table)
- A single separation at minimum current at -20°C in vacuum (for SN 011-018, light blue shaded area of the table)
- Random vibration test on the Serial Number 001 3U CubeSat in the NASA NLAS CubeSat dispenser (SN 011-014)A single separation in vacuum after soak at 11°C and transient to -1°C on the Serial Number 2 3U CubeSat (mechanism SN 015-018)

Table 5- Data taken from third generation flight devices (SN011-018)

Test #	Vacuum (Torr)	Current (A)	Voltage (V)	Power (W)	Tamb (°C)	Trel (°C)	ΔT (°C)	Δtime (s)	ΔT/Δt	Energy (W-s)	% Batt Energy	Interference Fit	Note
11.2	2.50E-02	2.60	7.28	18.9	21.8	81.3	59.5	46	1.29	870	0.54%	0.00055	
11.3	2.50E-02	2.60	7.28	18.9	21.0	77.7	56.7	48	1.18	909	0.56%	0.00055	
11.5	2.50E-02	2.60	7.28	18.9	19.6	86.9	67.3	45	1.50	852	0.53%	0.00055	
12.1	2.50E-02	2.60	7.28	18.9	21.0	85.0	64.0	53	1.21	1003	0.62%	0.0007	
13.1	2.50E-02	2.60	7.28	18.9	21.2	95.7	74.5	70	1.06	1325	0.82%	0.0007	
14.1	2.50E-02	2.60	7.28	18.9	21.0	79.0	58.0	50	1.16	946	0.59%	0.00045	
15.1	2.50E-02	2.60	7.28	18.9	21.4	79.6	58.2	55	1.06	1041	0.65%	0.00065	
15.2	1.40E-03	2.60	7.28	18.9	18.8	87.4	68.6	52	1.32	984	0.61%	0.00065	
16.1	2.50E-02	2.60	7.28	18.9	20.0	94.2	74.2	59	1.26	1117	0.69%	0.0007	
17.1	2.50E-02	2.60	7.28	18.9	20.5	91.8	71.3	58	1.23	1098	0.68%	0.0006	
18.1	2.50E-02	2.60	7.28	18.9	20.8	87.6	66.8	58	1.15	1098	0.68%	0.00065	
11.4	1.50E-05	2.16	6.05	13.1	-20	73.0	93.0	120	0.78	1568	0.97%	0.00055	
12.2	1.30E-06	2.16	6.05	13.1	-19.9	87.9	107.8	127	0.85	1659	1.03%	0.0007	
13.2	6.00E-06	2.16	6.05	13.1	-20	98.8	118.8	140	0.85	1829	1.13%	0.0007	
14.2	5.50E-06	2.16	6.05	13.1	-20.1	58.1	78.2	129	0.61	1685	1.04%	0.00045	
15.2	1.70E-06	2.16	6.05	13.1	-20.1	78.5	98.6	130	0.76	1698	1.05%	0.00065	
17.2	9.80E-06	2.16	6.05	13.1	-20	94.0	114.0	140	0.81	1829	1.13%	0.0006	
18.2	3.40E-06	2.16	6.05	13.1	-20			133		1737	1.08%	0.00065	
16.2	8.50E-07	2.16	6.05	13.1	-20.3			122		1594	0.99%	0.0007	
15.3	6.00E-06	2.19	8.06	17.6	-1.0	82.0	81.0	71	1.14	1252	0.78%	0.00065	
16.3	6.00E-06	2.16	8.00	17.3	-1.0	80.0	87.0	72	1.21	1243	0.77%	0.0007	
17.3	6.00E-06	2.17	7.92	17.2	-1.0	96.0	89.0	78	1.14	1342	0.83%	0.0006	
18.3	6.00E-06	2.14	7.90	16.9	-1.0	92.0	91.0	79	1.15	1335	0.83%	0.00065	
11.6	ATM	2.26	6.33	14.3	50			57		814	0.50%	0.00055	
12.3	ATM	2.26	6.33	14.3	50			63		900	0.56%	0.0007	
13.3	ATM	2.29	6.40	14.6	50			84		1228	0.76%	0.0007	5
14.3	ATM	2.23	6.25	14.0	50			59		824	0.51%	0.00045	

5	Automated shutdown failed because of a harness fabrication error. Manual shutdown was delayed.

We performed a basic analysis of the raw data from the **flight device (SN 011-018)** separations at ambient, cold vacuum (-20°C), thermal balance and thermal cycling cases. From these data, we determined the mean, standard deviation and two-sigma data, for time to separate, delta-T, and power required to separate.

The two-sigma time to separate is calculated as follows: $\mathbf{T_{2\sigma} = \textit{Mean} + (2 * \sigma)}$ where $\mathbf{T_{2\sigma}}$ is the 2 sigma time to separate, ***Mean*** is the arithmetic mean of the times to separate, and $\boldsymbol{\sigma}$ is the standard deviation between the times to separate.

We recommended to our team that 2 sigma durations be programmed to assure that timed separations are successful. Table 6 lists the data for the four cases analyzed (2.6 A at ambient temperature in vacuum, 2.16 A at -20°C in vacuum, ~2.15 A during thermal balance testing at 0°C, ~2.25 A during thermal cycling in ambient pressure at 50°C).

Table 6 – Rudimentary statistical analysis of CTERA temperature, time and energy data

Vacuum, 2.6A, 20°C			
	mean	std dev	X + 2σ
Time	54.0	7.2	68.4
dT	65.4	6.6	78.5
Energy	1022.1	136.0	1294.1
Vacuum, Thermal Balance, 2.15A, 0°C			
	mean	std dev	X + 2σ
Time	75.0	4.1	83.2
dT	87.0	4.32	95.6
Energy	1292.8	52.8	1398.4

Vacuum 2.16 A, -20°C			
	mean	std dev	X + 2σ
Time	130.1	7.4	144.9
dT	101.7	15.0	131.6
Energy	1699.9	96.6	1893.1
Ambient, Thermal Cyclling, 2.25A, 50°C			
	mean	std dev	X + 2σ
Time	65.8	12.4	90.6
dT			
Energy	941.6	194.8	1331.2

We had already confirmed that actuation in vacuum reduces the energy required to actuate (see the difference between test 4.1 and tests 4.2-4.10). Looking further at the data, we noticed a correlation between input power and time to separate, and a correlation between initial temperature and time to separate. The following several figures pictorially represent relationships between initial temperature, delta-T, time, power level, and the different interference fits of the various actuators. The left chart of Figure 9 shows that release time is directly related to the energy expended, as one would expect. It also shows a correlation between the power applied to the device, illustrated here by various current levels, and time to release. The faster energy is applied to the device (more power), the less time and energy it takes to operate. The right chart of Figure 9 shows the relationship between release delta-T and power. As power increases, release delta-T decreases. It appears as the power applied to the high CTE part is increased, its rate of expansion is higher and less heat is applied to the low CTE part. Since less heat is applied to the low CTE part, it expands less and more slowly, resulting in a lower delta-T before the parts separate.

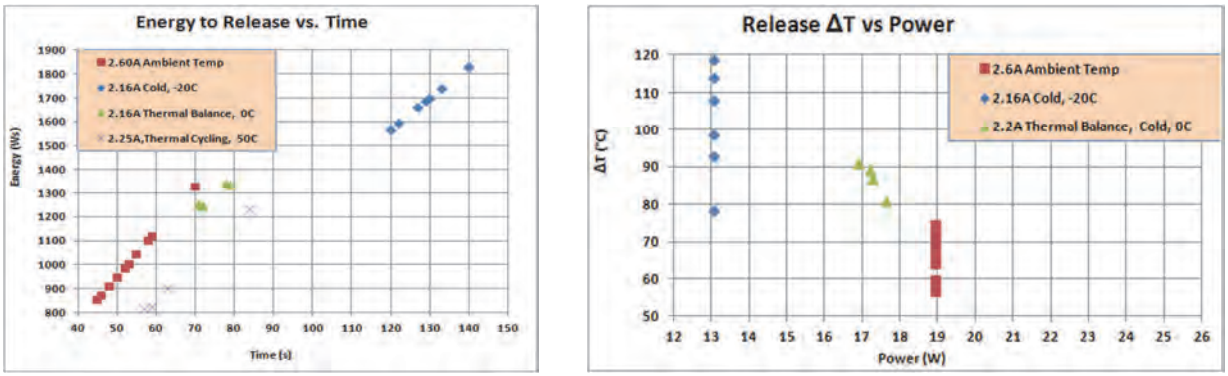

Figure 9 – Strong relationships between energy, delta-T, and time to separate

The left chart of Figure 10 shows the effect the interference fit has upon the delta-T required for the parts to separate. As the analytical model suggests, the looser fit requires less delta-T for the parts to separate. The right chart of Figure 10 shows the effect the interference fit has upon the energy required to separate. The high CTE part doesn't need to expand as much to free the low CTE part, which takes less energy. Additionally, when the interface pressure between the two parts is lower, less conductive heat transfer results between the two parts, so less energy is wasted heating the low CTE part. We initially expected less scatter in these charts, but realized static friction effects cause scatter (torque vs. preload tests exhibit this scatter, for example), and that minute surface imperfections have an appreciable affect on results, since the interface pressures are quite high in this design. These two charts also show two other relationships. The first, which we already discussed, is between input power and the time, energy, and delta-T required for separation. The second, discussed in the following paragraph, is the relationship between the initial temperature and the time, energy and delta-T required for separation.

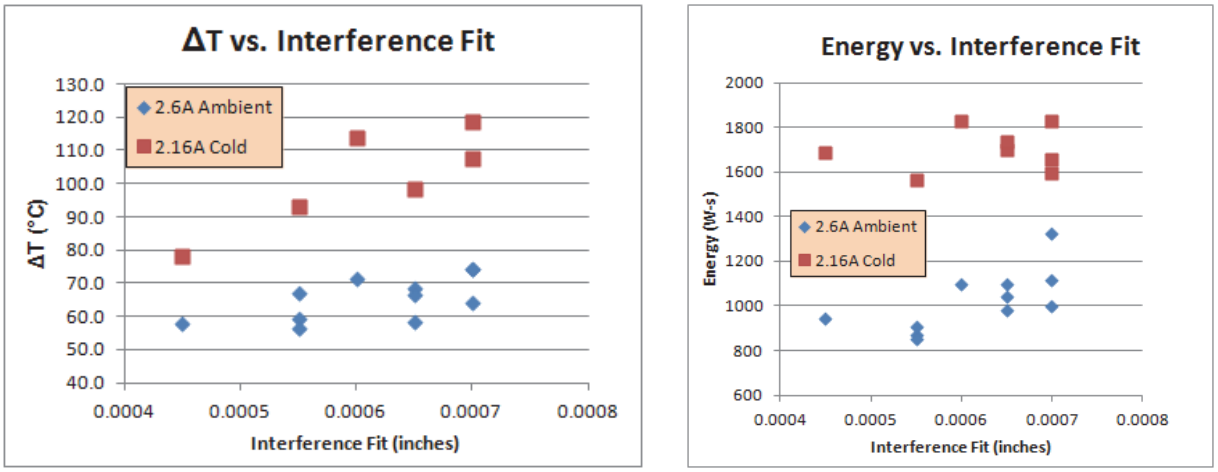

Figure 10 – Relationships between interference fit, delta-T and energy required to separate

The left chart of Figure 11 shows the relationship between the initial temperature and the energy required to separate. The right chart of Figure 11 shows the relationship between actuation delta-T and the initial temperature. Since the parts were manufactured at 20°C, they will have a tighter interference fit with a lower initial temperature and will have a looser interference fit as they have a higher initial temperature.

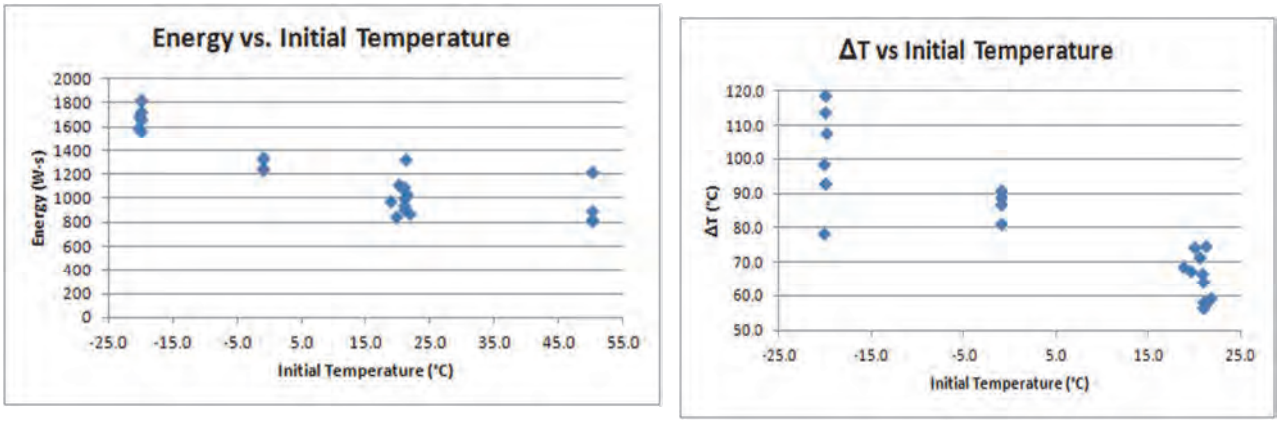

Figure 11 – Relationships between initial temperature, and energy to actuate

Testing of the flight parts has thus far confirmed the following:

- A single CTERA has been shown to not degrade in performance over 10 cycles. We intend to perform further life testing when given the opportunity.

- Despite variability in interference fits from device to device, actuation data are tightly grouped and can be used, when factored, for timed separation commands when the bus is at room temperature in vacuum.
- The tell-tale function of the actuators was determined to be reliable though the vibration testing and subsequent thermal cycling testing they underwent.
- Tell-tale reliability is not affected by vibration or thermal cycling.
- Operating condition effects:
    - The effect of supplied current on total energy and "on-time" is significant.
    - The effect of initial temperature on actuation times is also significant.
    - Since the "on-time" can vary wildly with initial temperature and supplied current, these devices should not be used open loop to avoid damaging the heaters. We recommend either: implement tell-tale reading circuits, as APL's CubeSat did, or implement temperature sensors with each actuator and shut the devices off when the devices reach the maximum allowable temperature, or code in a two dimensional look-up table in the flight software, which sets "on-time" as a function of battery state of charge (resulting in current delivered to the device) and initial temperature.

Lessons Learned

- Don't skimp on Ground Support Equipment (GSE) and test equipment. Test GSE are just as important as the flight hardware:
    - It would have been immediately obvious that the first (and second) generation devices were incompatible with the CubeSat solar array deployment motion if we had tested with a flight-like wing mechanism from the beginning. Representing boundary conditions correctly would have saved one design iteration.
    - Pay attention to data acquisition. We lost some data due to shortcuts in setting up the data acquisition system. We also would have been able to capture more data (such as temperature vs time curves) with a more advanced data acquisition system.
    - We could have saved money and time by testing more than one device at a time with more elaborate GSE
    - Enlist subject matter experts initially. We could have eliminated one design revision if we had known of electrical parts de-rating guidelines and selected the right resistors in the beginning.
- Incremental development is cost effective. By making really cheap parts, testing a little and learning a lot, fabricating a slightly more elaborate second generation device, testing a little and learning a lot more, we were still able to develop and test the flight device in a short, inexpensive effort.
- Manufacturing methods are critical to the success of a mechanism design; it wouldn't have cost much more to fabricate the first generation parts on the newer generation CNC lathe, rather than the manually operated lathe.

Conclusion

A compact device for releasing deployable structures has been developed exploiting differential coefficients of thermal expansion of two dissimilar materials. The resultant device is economical, miniature, simple in concept and execution, uses little power, produces negligible shock, is easily re-settable, and is able to restrain a relatively large load, considering its size. Through a total of 37 test actuations, the third generation design demonstrated a robust device that performed reliably in a flight-like environment. This device is applicable to small deployable devices on instruments, CubeSats and Nanosatellites, and has the capability to be used as an initiation device for mechanisms used on conventional spacecraft and larger instruments. Future work will focus on alternate materials, such as invar, which has a very low CTE, and manufacturing processes, as well as integration into larger load capacity mechanisms.